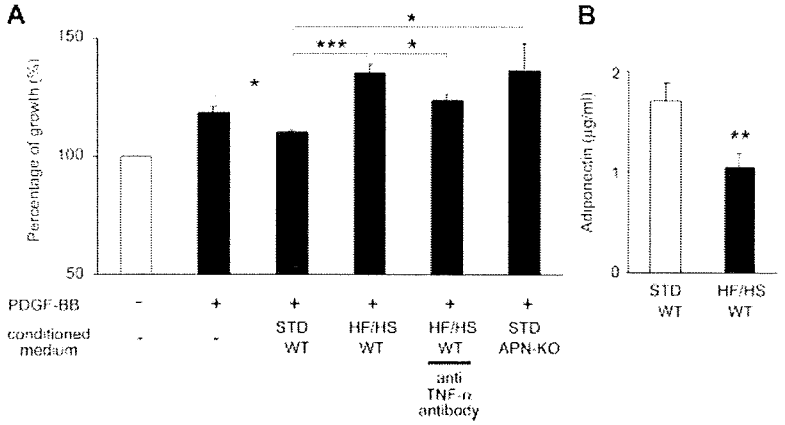

Figure 4. The effect of conditioned medium from subcutaneous fat of STD and HF/HS mice on SMCs. A, Number of SMCs (percentage of growth) was evaluated by MTS assay. The conditioned medium from the subcutaneous fat of STD mice (WT), but not of HF/HS mice (WT), attenuated increased SMCs number induced by PDGF-BB (10 ng/mL). The conditioned medium of HF/HS fat increased SMC number. Pretreatment of anti-TNF-α antibody suppressed the increased SMCs number. The conditioned medium from the subcutaneous fat of APN-deficient mice increased SMCs number compared with conditioned medium from STD subcutaneous fat. B, APN protein levels were significantly higher in the conditioned medium from STD mice than in that from HF/HS mice. The data from 3 independent experiments are shown as means±SEM. $^*P<0.05$, $^{**}P<0.01$, $^{***}P<0.001$.

ating the initiation and progression of vascular lesion formation.[23–25] In contrast to these well-characterized processes within the vessel wall, changes in the adventitia during vascular remodeling have been largely neglected.

The adventitial and periadventitial tissues are composed of various cell types including adipocytes, vascular cells, macrophages, T cells, mast cells, and fibroblasts.[26–30] It was demonstrated that perivascular adventitial adipose tissue releases a transferable adventitia-derived relaxing factor that acts by tyrosine kinase–dependent activation of K^+ channels in vascular SMCs.[31] Recent reports showed that periadventitial fat secretes various kinds of chemokines and might contribute to the progression of obesity-associated atherosclerosis.[32] Epicardial adipose tissue has been reported to be a source of inflammatory mediators[33] and is an indicator of cardiovascular risk.[34] Quite recently, Chatterjee et al reported that perivascular adipocytes exhibit reduced differentiation and proinflammatory state, suggesting that dysfunction of perivascular adipose tissues induced by fat feeding may link metabolic signals to inflammation in the blood vessel wall.[35] Patients with obesity[14] and coronary artery disease[36] have low plasma APN levels. It was suggested that perivascular adipocytes loose activities to secrete APN in obesity, leading to hypoxia, inflammation, and oxidative stress.[37] These results suggested that perivascular fat may play a role in increased risk of cardiovascular disease in obese individuals. However, the physiological and/or pathological role of perivascular adipose tissue in the maintenance of vascular homeostasis and in pathological vascular remodeling remains to be elucidated.[31]

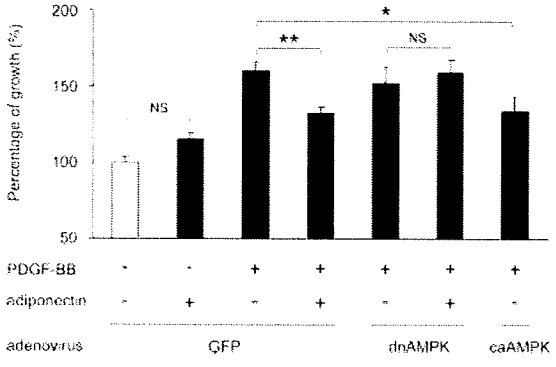

Figure 5. APN suppresses the PDGF-BB–induced increased SMC numbers through AMPK. Number of SMCs (percentage of growth) was evaluated by MTS assay. Pretreatment with APN suppressed the increased SMC numbers induced by PDGF-BB (20 ng/mL) but did not modify SMC numbers without PDGF-BB. Transduction with dn-AMPK reversed the suppressive effects of APN on increased SMCs number induced by PDGF-BB. In contrast, transduction with ca-AMPK suppressed increased SMC numbers induced by PDGF-BB. The data from 3 independent experiments are shown as means±SEM. $^*P<0.05$, $^{**}P<0.01$.

In this study, we provide direct evidence that perivascular fat may protect against neointimal formation after angioplasty under physiological conditions and that inflammatory changes in the periadventitial fat may have a direct role in the pathogenesis of vascular disease accelerated by obesity. It was suggested that APN secreted from perivascular fat may play a protective role in neointima formation of the adjacent artery in situ after vascular injury in lean mice.

We made efforts to transplant periadventitial fat from one blood vessel to the other. However, it was impossible to obtain enough amount of periadventitial fat for the transplantation to coat the artery of another mouse. Alternatively, in this study, we implanted subcutaneous or visceral fat from other mice around the wire-injured femoral artery after removal of endogenous perivascular fat. Our experiments using subcutaneous or visceral fat transplantation from the mice fed on STD or HF/HS diet successfully demonstrated the importance of adipose tissues in perivascular area in regulating neointima formation in the injured vessel via paracrine effects of adipocytokines. Consist with notion, local delivery, but not systemic administration, of APN to perivascular area effectively inhibited neointima formation.

In summary, we provide direct evidence that obesity increases periadventitial adipose tissue inflammation and may contribute to pathological vascular remodeling in response to injury. Our findings support the notion that changes in periadventitial adipose tissue may have a role in obesity-associated cardiovascular complications. The results described here suggest the previously unappreciated role of periadventitial fat in the regulation of vascular remodeling.

Sources of Funding

This study was supported in part by the Program for Promotion of Basic and Applied Researches for Innovations in Bio-oriented Industry and by grants from the Ministry of Education, Culture, Sports, Science and Technology of Japan (Knowledge Cluster and New Research Area).

Disclosures

None.

References

1. Calle EE, Thun MJ, Petrelli JM, Rodriguez C, Heath CW Jr. Body-mass index and mortality in a prospective cohort of U.S. adults. *N Engl J Med.* 1999;341:1097–1105.
2. Flegal KM, Carroll MD, Ogden CL, Johnson CL. Prevalence and trends in obesity among US adults, 1999–2000. *JAMA.* 2002;288:1723–1727.
3. James PT, Rigby N, Leach R. The obesity epidemic, metabolic syndrome and future prevention strategies. *Eur J Cardiovasc Prev Rehabil.* 2004; 11:3–8.
4. Adams KF, Schatzkin A, Harris TB, Kipnis V, Mouw T, Ballard-Barbash R, Hollenbeck A, Leitzmann MF. Overweight, obesity, and mortality in a large prospective cohort of persons 50 to 71 years old. *N Engl J Med.* 2006;355:763–778.
5. Lakka TA, Lakka HM, Salonen R, Kaplan GA, Salonen JT. Abdominal obesity is associated with accelerated progression of carotid atherosclerosis in men. *Atherosclerosis.* 2001;154:497–504.
6. Kenchaiah S, Evans JC, Levy D, Wilson PW, Benjamin EJ, Larson MG, Kannel WB, Vasan RS. Obesity and the risk of heart failure. *N Engl J Med.* 2002;347:305–313.
7. Brook RD. Obesity, weight loss, and vascular function. *Endocrine.* 2006; 29:21–25.
8. Hubert HB, Feinleib M, McNamara PM, Castelli WP. Obesity as an independent risk factor for cardiovascular disease: a 26-year follow-up of participants in the Framingham Heart Study. *Circulation.* 1983;67: 968–977.
9. Van Gaal LF, Mertens IL, De Block CE. Mechanisms linking obesity with cardiovascular disease. *Nature.* 2006;444:875–880.
10. Nikolsky E, Kosinski E, Mishkel GJ, Kimmelstiel C, McGarry TF Jr, Mehran R, Leon MB, Russell ME, Ellis SG, Stone GW. Impact of obesity on revascularization and restenosis rates after bare-metal and drug-eluting stent implantation (from the TAXUS-IV trial). *Am J Cardiol.* 2005;95: 709–715.
11. Yudkin JS, Stehouwer CD, Emeis JJ, Coppack SW. C-reactive protein in healthy subjects: associations with obesity, insulin resistance, and endothelial dysfunction: a potential role for cytokines originating from adipose tissue? *Arterioscler Thromb Vasc Biol.* 1999;19:972–978.
12. Thogersen AM, Jansson JH, Boman K, Nilsson TK, Weinehall L, Huhtasaari F, Hallmans G. High plasminogen activator inhibitor and tissue plasminogen activator levels in plasma precede a first acute myocardial infarction in both men and women: evidence for the fibrinolytic system as an independent primary risk factor. *Circulation.* 1998;98: 2241–2247.
13. Malavazos AE, Cereda E, Morricone L, Coman C, Corsi MM, Ambrosi B. Monocyte chemoattractant protein 1: a possible link between visceral adipose tissue-associated inflammation and subclinical echocardiographic abnormalities in uncomplicated obesity. *Eur J Endocrinol.* 2005;153: 871–877.
14. Arita Y, Kihara S, Ouchi N, Takahashi M, Maeda K, Miyagawa J, Hotta K, Shimomura I, Nakamura T, Miyaoka K, Kuriyama H, Nishida M, Yamashita S, Okubo K, Matsubara K, Muraguchi M, Ohmoto Y, Funahashi T, Matsuzawa Y. Paradoxical decrease of an adipose-specific protein, adiponectin, in obesity. *Biochem Biophys Res Commun.* 1999; 257:79–83.
15. Maeda N, Shimomura I, Kishida K, Nishizawa H, Matsuda M, Nagaretani H, Furuyama N, Kondo H, Takahashi M, Arita Y, Komuro R, Ouchi N, Kihara S, Tochino Y, Okutomi K, Horie M, Takeda S, Aoyama T, Funahashi T, Matsuzawa Y. Diet-induced insulin resistance in mice lacking adiponectin/ACRP30. *Nat Med.* 2002;8:731–737.
16. Sata M, Saiura A, Kunisato A, Tojo A, Okada S, Tokuhisa T, Hirai H, Makuuchi M, Hirata Y, Nagai R. Hematopoietic stem cells differentiate into vascular cells that participate in the pathogenesis of atherosclerosis. *Nat Med.* 2002;8:403–409.
17. Sata M, Maejima Y, Adachi F, Fukino K, Saiura A, Sugiura S, Aoyagi T, Imai Y, Kurihara H, Kimura K, Omata M, Makuuchi M, Hirata Y, Nagai R. A mouse model of vascular injury that induces rapid onset of medial cell apoptosis followed by reproducible neointimal hyperplasia. *J Mol Cell Cardiol.* 2000;32:2097–2104.
18. Takaoka M, Uemura S, Kawata H, Imagawa K, Takeda Y, Nakatani K, Naya N, Horii M, Yamano S, Miyamoto Y, Yoshimasa Y, Saito Y. Inflammatory response to acute myocardial infarction augments neointimal hyperplasia after vascular injury in a remote artery. *Arterioscler Thromb Vasc Biol.* 2006;26:2083–2089.
19. Tabata Y, Ikada Y. Vascularization effect of basic fibroblast growth factor released from gelatin hydrogels with different biodegradabilities. *Biomaterials.* 1999;20:2169–2175.
20. Nagata D, Takeda R, Sata M, Satonaka H, Suzuki E, Nagano T, Hirata Y. AMP-activated protein kinase inhibits angiotensin II-stimulated vascular smooth muscle cell proliferation. *Circulation.* 2004;110:444–451.
21. Nagata D, Kiyosue A, Takahashi M, Satonaka H, Tanaka K, Sata M, Nagano T, Nagai R, Hirata Y. A new constitutively active mutant of AMP-activated protein kinase inhibits anoxia-induced apoptosis of vascular endothelial cell. *Hypertens Res.* 2009;32:133–139.
22. Matsuda M, Shimomura I, Sata M, Arita Y, Nishida M, Maeda N, Kumada M, Okamoto Y, Nagaretani H, Nishizawa H, Kishida K, Komuro R, Ouchi N, Kihara S, Nagai R, Funahashi T, Matsuzawa Y. Role of adiponectin in preventing vascular stenosis. The missing link of adipo-vascular axis. *J Biol Chem.* 2002;277:37487–37491.
23. Ross R. Atherosclerosis–an inflammatory disease. *N Engl J Med.* 1999; 340:115–126.
24. Serrano CV Jr, Ramires JA, Venturinelli M, Arie S, D'Amico E, Zweier JL, Pileggi F, da Luz PL. Coronary angioplasty results in leukocyte and platelet activation with adhesion molecule expression. Evidence of inflammatory responses in coronary angioplasty. *J Am Coll Cardiol.* 1997;29:1276–1283.
25. Libby P. Inflammation in atherosclerosis. *Nature.* 2002;420:868–874.
26. Sartore S, Chiavegato A, Faggin E, Franch R, Puato M, Ausoni S, Pauletto P. Contribution of adventitial fibroblasts to neointima formation and vascular remodeling: from innocent bystander to active participant. *Circ Res.* 2001;89:1111–1121.
27. Shi Y, O'Brien JE, Fard A, Mannion JD, Wang D, Zalewski A. Adventitial myofibroblasts contribute to neointimal formation in injured porcine coronary arteries. *Circulation.* 1996;94:1655–1664.
28. Li G, Chen YF, Kelpke SS, Oparil S, Thompson JA. Estrogen attenuates integrin-beta(3)-dependent adventitial fibroblast migration after inhibition of osteopontin production in vascular smooth muscle cells. *Circulation.* 2000; 101:2949–2955.
29. Okamoto E, Couse T, De Leon H, Vinten-Johansen J, Goodman RB, Scott NA, Wilcox JN. Perivascular inflammation after balloon angioplasty of porcine coronary arteries. *Circulation.* 2001;104:2228–2235.
30. Bot I, de Jager SC, Zernecke A, Lindstedt KA, van Berkel TJ, Weber C, Biessen EA. Perivascular mast cells promote atherogenesis and induce plaque destabilization in apolipoprotein E-deficient mice. *Circulation.* 2007;115:2516–2525.
31. Lohn M, Dubrovska G, Lauterbach B, Luft FC, Gollasch M, Sharma AM. Periadventitial fat releases a vascular relaxing factor. *FASEB J.* 2002;16: 1057–1063.
32. Henrichot E, Juge-Aubry CE, Pernin A, Pache JC, Velebit V, Dayer JM, Meda P, Chizzolini C, Meier CA. Production of chemokines by perivascular adipose tissue: a role in the pathogenesis of atherosclerosis? *Arterioscler Thromb Vasc Biol.* 2005;25:2594–2599.
33. Mazurek T, Zhang L, Zalewski A, Mannion JD, Diehl JT, Arafat H, Sarov-Blat L, O'Brien S, Keiper EA, Johnson AG, Martin J, Goldstein BJ, Shi Y. Human epicardial adipose tissue is a source of inflammatory mediators. *Circulation.* 2003;108:2460–2466.
34. Iacobellis G, Ribaudo MC, Assael F, Vecci E, Tiberti C, Zappaterreno A, Di Mario U, Leonetti F. Echocardiographic epicardial adipose tissue is related to anthropometric and clinical parameters of metabolic syndrome: a new indicator of cardiovascular risk. *J Clin Endocrinol Metab.* 2003; 88:5163–5168.
35. Chatterjee TK, Stoll LL, Denning GM, Harrelson A, Blomkalns AL, Idelman G, Rothenberg FG, Neltner B, Romig-Martin SA, Dickson EW, Rudich S, Weintraub NL. Proinflammatory phenotype of perivascular adipocytes: influence of high-fat feeding. *Circ Res.* 2009;104:541–549.
36. Kumada M, Kihara S, Sumitsuji S, Kawamoto T, Matsumoto S, Ouchi N, Arita Y, Okamoto Y, Shimomura I, Hiraoka H, Nakamura T, Funahashi T, Matsuzawa Y. Association of hypoadiponectinemia with coronary artery disease in men. *Arterioscler Thromb Vasc Biol.* 2003;23:85–89.
37. Greenstein AS, Khavandi K, Withers SB, Sonoyama K, Clancy O, Jeziorska M, Laing I, Yates AP, Pemberton PW, Malik RA, Heagerty AM. Local inflammation and hypoxia abolish the protective anticontractile properties of perivascular fat in obese patients. *Circulation.* 2009;119:1661–1670.

Material and Methods

Immunohistochemical staining

Paraffin-embedded sections (4-μm thick) were deparaffinized and blocked using 2% rabbit or horse serum. The sections were then incubated with anti-CD31 antibody (BD Pharmingen), followed by incubation with avidin-biotin complex and Vector Red substrate (Vector Laboratories). Sections were counterstained with hematoxylin.

Online supplement Figure I

Fat transplantation induced neovascularisation around the artery

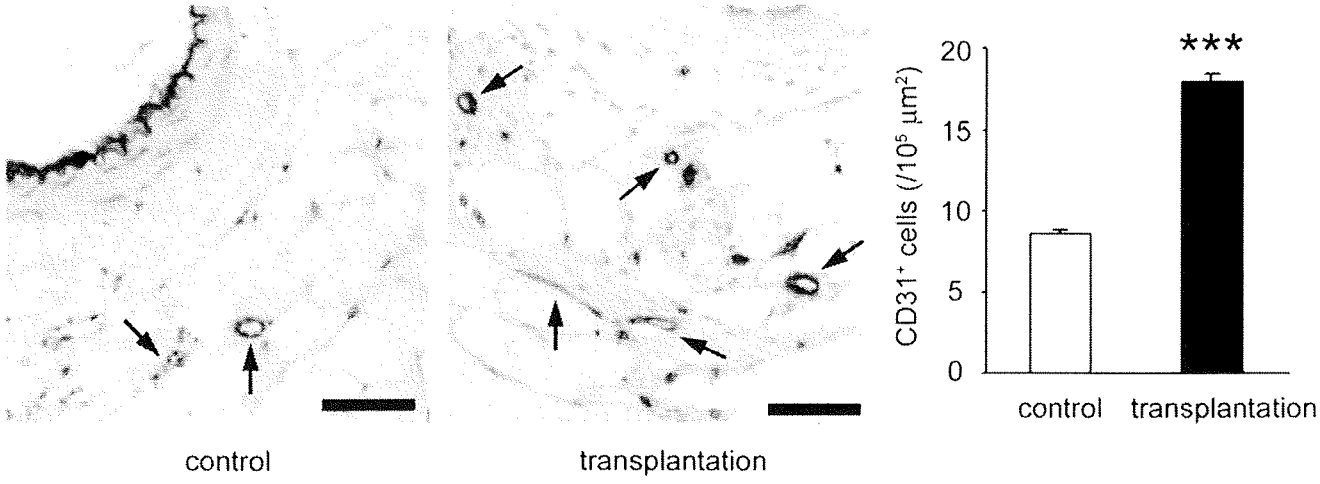

Fat transplantation induced accumulation of vascular endothelial cells around the artery. Immunohistochemical analysis showed accumulation of CD31-positive vascular endothelial cells (arrows) within periadventitia in fat transplantation mice at one week. Scale bar, 50 μm. Results are expressed as mean ± S.E.M. ***P<0.01. n=6.

Online supplement Figure II

Transplantation of subcutaneous or visceral fat from standard chow diet (STD) or high fat high sucrose diet (HF/HS) mice after removal of perivascular adipose tissue

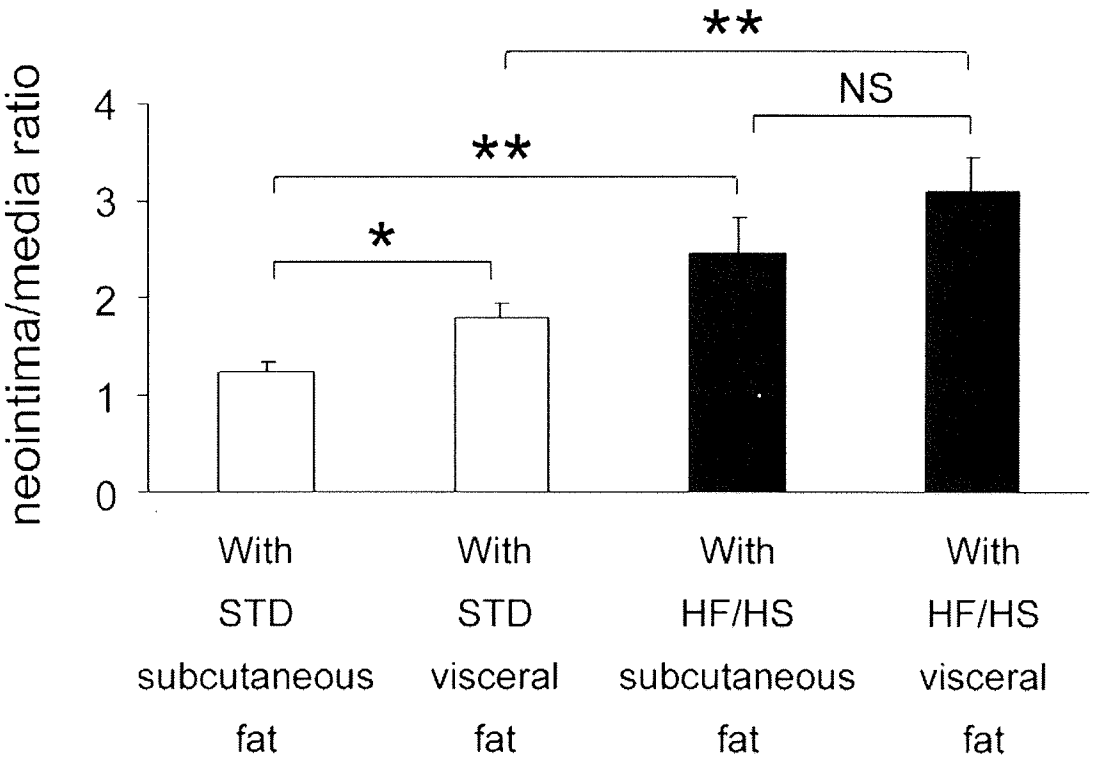

Morphometric analysis of injured femoral arteries at 4 weeks. Subcutaneous or visceral fat from STD (n=6 each) or HF/HS mice (n=6 each) was transplanted after removal of endogenous periadventitial adipose tissue. Results are expressed as mean ± S.E.M. *P<0.05, **P<0.01, NS, not statistically significant.

Online supplement Figure III

Obese and visceral fat induced inflammatory changes in adipose tissue

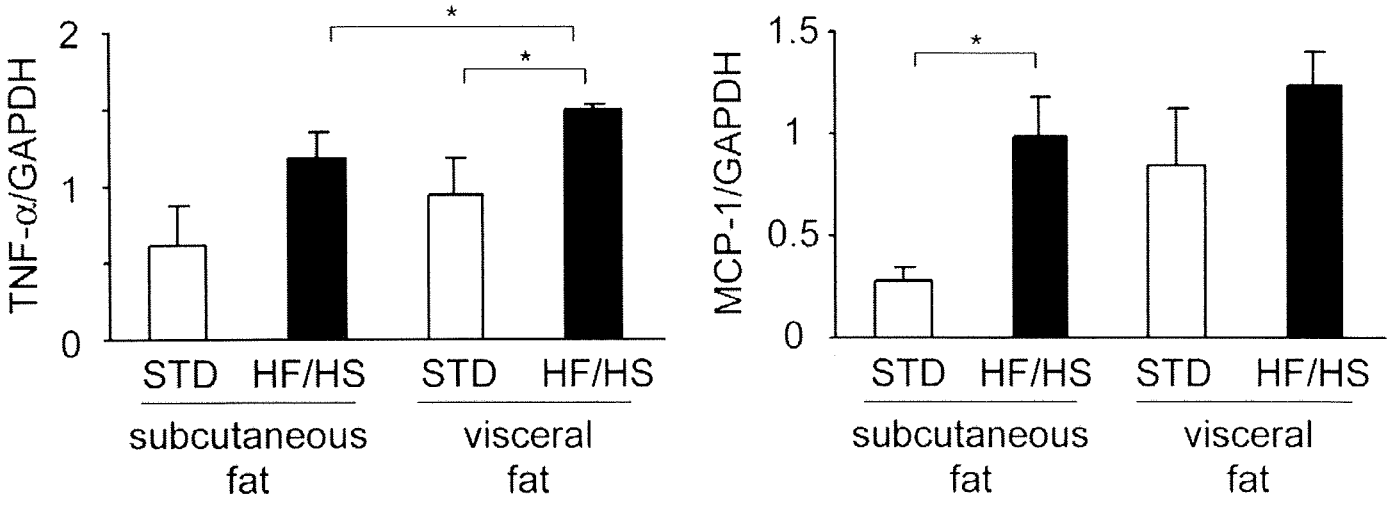

Expression of mRNA in subcutaneous and visceral fat from STD (n=3 each) and HF/HS (n=3 each) wild-type C57BL6 mice. Expression level was assessed by real-time PCR normalized to GAPDH level. Results are expressed as mean ± S.E.M. *P<0.05. STD, standard chow diet. HF/HS, high fat high sucrose diet.

Circ J 2009; **73:** 2300–2307

Long-Term Follow-up of Neointimal Coverage of Sirolimus-Eluting Stents

— Evaluation With Optical Coherence Tomography —

Ken-ichi Ishigami, MD; Shiro Uemura, MD; Yoshinobu Morikawa, MD; Tsunenari Soeda, MD; Satoshi Okayama, MD; Taku Nishida, MD; Yasuhiro Takemoto, MD; Kenji Onoue, MD; Satoshi Somekawa, MD; Yukiji Takeda, MD; Hiroyuki Kawata, MD; Manabu Horii, MD; Yoshihiko Saito, MD

Background: Late stent thrombosis related to delayed neointimal growth is a major concern after drug-eluting stent (DES) implantation. The time course of neointimal growth and risk factors of uncovered stent struts after sirolimus-eluting stent (SES) was studied using optical coherence tomography (OCT).

Methods and Results: The 60 patients were enrolled and classified into G1 (follow-up period <9 months, n=27), G2 (9–24 months, n=18), and G3 (>25 months, n=15). The time elapsed since SES implantation was associated with a significant increase in mean neointimal area and neointimal thickness, and also with a significant decrease in the number of uncovered stent struts (G1: 14.8%, G2: 11.7%, and G3: 4.1%, P<0.001). However, only 17.6% of implanted SES was completely covered by neointima, even in the G3 period. Small-diameter SES, complex coronary lesions with lipid and calcium content adjacent to stent struts, and diabetes predicted delayed neointimal coverage of SES struts in G1.

Conclusions: Neointima inside SES progressively increases after the routine follow-up period, but only a few SES were completely covered at 3 years after implantation. OCT is a useful modality for assessing neointimal formation after SES implantation, and may give important information about the strategy of antiplatelet therapy after DES implantation. (*Circ J* 2009; **73:** 2300–2307)

Key Words: Antiplatelet therapy; Drug-eluting stents; Optical coherence tomography; Thrombosis

Recent clinical trials have proved that drug-eluting stents (DES) inhibit neointimal proliferation and reduce the risk of in-stent restenosis.[1,2] However, there have been major concerns regarding the potential development of late stent thrombosis related to delayed neointimal formation over the struts of the DES and the discontinuation of dual antiplatelet therapy.[3] Although the incidence of DES thrombosis is reported to be less than 1%,[4–8] the incidence of death or myocardial infarction associated with this thrombosis is greater than 60%,[9] and related mortality rates range from 20% to 45%.[6,10] In 2008, the AHA/ACC/SCAI recommended that dual antiplatelet drug therapy should continue for at least 12 months after DES implantation if patients are not at high risk of bleeding,[11] longer than had previously been suggested. In order to establish guidelines for the safe cessation of antiplatelet therapy after DES implantation, a large randomized clinical trial should be performed. Furthermore, it seems important to know whether adequate neointimal coverage of DES has been achieved before stopping dual antiplatelet therapy, especially the thienopyridines. With this clinical perspective, several intravascular ultrasound (IVUS) studies have sought to evaluate the neointimal coverage of sirolimus-eluting stent (SES), but they have revealed that IVUS is unable to detect the neointimal layers covering the struts of most DES, even at long-term follow-up, because of its relatively low spatial resolution.[12]

Editorial p2210

Intravascular optical coherence tomography (OCT) is a newly developed intravascular imaging modality with a maximal spatial resolution of 10μm,[13–15] which is approximately 10-fold higher than that of IVUS. The aim of the present study was to use intravascular OCT to analyze the time course of neointimal coverage of SES in the chronic phase, and to identify the predictive factors influencing delayed neointimal coverage of stent struts.

Methods

Study Population

From September 2006 to January 2009, we enrolled 60 patients (50 men, 10 women) with coronary artery disease

Received December 2, 2008; revised manuscript received June 30, 2009; accepted August 4, 2009; released online September 29, 2009

First Department of Medicine, Nara Medical University, Kashihara, Japan

Grant support: none.

Mailing address: Shiro Uemura, MD, First Department of Medicine, Nara Medical University, 840 Shijo-cho, Kashihara 634-0813, Japan.
E-mail: suemura@naramed-u.ac.jp

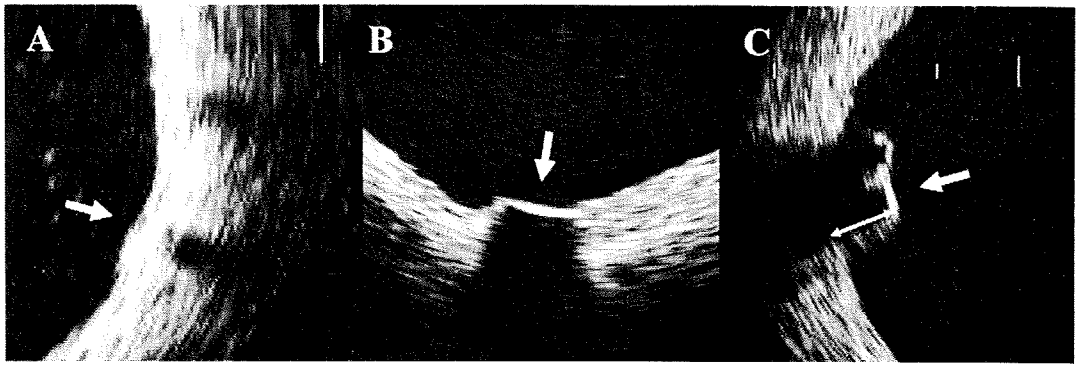

Figure 1. OCT images of strut apposition and neointimal coverage of a sirolimus-eluting stent. (**A**) Strut apposing the vessel wall and covered by neointimal tissue. (**B**) Strut apposing the vessel wall, but not covered by neointimal tissue. (**C**) Strut not apposing the vessel wall (arrows). Bidirectional arrow indicates the distance between the center reflection of the strut and the internal margin of the vessel wall just behind the strut. Arrows indicate the struts.

who had previously received SES in native coronary arteries. At the time of SES implantation, the endpoint of deployment was determined by angiography. All patients enrolled in this study underwent routine angiographic follow-up within 8 months after SES implantation, and 27 patients also underwent OCT study at that time. The remaining 33 patients voluntarily underwent an OCT study and concomitant second coronary angiography from several months to 43 months after the completion of the first follow-up angiography by accepting the purpose of the present study. None of the patients underwent OCT study more than twice. Patients were excluded from the study if they had left main or ostial coronary lesions, congestive heart failure, or renal insufficiency with baseline serum creatinine >2.0 mg/dl.

Patients were classified into 3 subgroups according to time since SES implantation: G1 (<9 months, 27 patients), G2 (9–24 months, 18 patients) and G3 (25–43 months, 15 patients). All patients were taking aspirin (100 mg/day) and ticlopidine (200 mg/day) for at least 8 months after SES implantation, after which all patients were taking aspirin 100 mg/day, except 1 patient in the G3 group who was taking only ticlopidine.

For the purpose of assessing coronary risk factors, hypertension was considered to be present if a patient's blood pressure was >140/90 mmHg, or antihypertensive medication was being taken. Diabetes mellitus was considered present if the patient was taking glucose-lowering medications or insulin, or the fasting plasma glucose concentration was >126 mg/dl. Dyslipidemia was considered to be present if a patient's low-density lipoprotein level was >120 mg/dl or the patient was taking statins.

This study was approved by the Ethical Committee of Nara Medical University (2006–2020), and written informed consent was given by each patient.

Angiographic and OCT Image Acquisition

The OCT system used in the present study has been described previously.[16] After routine coronary angiography, an intravascular OCT catheter (ImageWire, LightLab Imaging, Westford, MA, USA) was inserted through a 6 or 7Fr guiding catheter into the target coronary arteries beyond the implanted SES. After complete vasodilatation of the coronary artery by nitroglycerin (0.5 mg), OCT images were recorded during continuous infusion of Lactated Ringer's solution at 0.5 ml/s through the occlusion catheter (OBC, LightLab Imaging) in order to remove blood from the field of view and allow clear visualization of the vessel wall. The coronary occlusion time for each OCT imaging was less than 40 s. Serial OCT images were obtained using an automatic pullback device at a rate of 1.0 mm/s. The images were processed and analyzed using proprietary software from LightLab Imaging.

OCT Data Analysis

OCT images were analyzed by 2 independent observers who did not know the patients' clinical background or angiographic lesion characteristics. For the assessment of neointimal coverage of stent struts, cross-sectional OCT images were obtained at 1-mm intervals (every 15 frames) from the distal to proximal ends of each implanted SES. For each cross-sectional OCT image, the surface of every strut was examined and then classified into 1 of 3 categories: (1) strut apposing vessel wall and covered by neointimal tissue, (2) strut apposing vessel wall, but not covered by neointimal tissue, or (3) strut not apposing vessel wall (malapposition). Because the thickness of the SES struts is 140 μm, and the maximal spatial resolution of OCT ranges from 10 to 30 μm, malapposition of the stent strut to the vessel wall was defined as the presence of more than 170 μm between the center reflection of the strut and the internal margin of the vessel wall just behind the strut. We excluded segments that overlapped or were located in side branches, and also images with poor quality. Representative OCT images are shown in **Figures 1A–C**.

For each implanted SES, planimetric measurement of neointimal thickness (NIT) and area (NIA) within the SES was performed. NIT and NIA were measured every 1 mm from the distal to the proximal ends of each SES. Stent area and lumen area in every image were measured by manual tracing.

We also evaluated the tissue characteristics of the vascular wall attached to the SES strut every 1 mm from the distal to the proximal ends of each SES. Because the image just behind strut was impossible to determine because of the shadow artifact of the strut, tissue characteristics adjacent to the edge of the shadow artifact were analyzed and classified into 1 of 3 categories: (1) intimal layer consisting of simple fibrous tissue, (2) intimal layer containing lipid and fibrous tissue, and (3) intimal layer containing calcification and fibrous tissue. Discernment of specific tissues with OCT was accomplished using the definitions of Kume

Table 1. Patients' Baseline Characteristics

	G1 (5–8 months)	G2 (9–24 months)	G3 (25–43 months)	P value
Clinical background				
No. of patients	27	18	15	
Time to OCT procedure (months)	7.1±0.8	13.8±3.6	32.6±5.6	
Age, years	65.0±10.4	63.4±9.6	65.1±10.3	0.52
Men (%)	21 (77.8%)	15 (83.3%)	14 (93.3%)	0.43
ACS (%)	4 (14.8%)	3 (16.7%)	3 (20.0%)	0.91
Risk factors				
Dyslipidemia, n (%)	16 (59.3%)	12 (66.7%)	9 (60.0%)	0.87
Hypertension,* n (%)	16 (59.3%)	12 (66.7%)	9 (60.0%)	0.87
Diabetes mellitus,† n (%)	13 (48.1%)	9 (50.0%)	8 (53.3%)	0.94
Smoking, n (%)	16 (59.3%)	12 (66.7%)	8 (53.3%)	0.73
HDL-cholesterol (mg/dl)	54±16	52±16	49±15	0.60
LDL-cholesterol (mg/dl)	121±29	108±25	110±30	0.26
Triglyceride (mg/dl)	117±45	112±52	98±36	0.49
Procedural background				
No. of stents	28	21	17	
LAD/LCX/RCA, (n)	15/10/3	12/4/5	6/4/7	0.15
AHA type of lesion				
A/B1, (n)	1/8	0/5	0/7	
B2/C, (n)	12/7	10/6	6/4	
Stent diameter (mm)	2.75±0.29	2.97±0.34	2.85±0.36	0.10
Stent length (mm)	20.4±5.32	22.9±5.28	20.5±5.10	0.21
Max. inflation pressure (atm)	18.4±3.73	16.8±4.20	18.1±3.90	0.59

*Defined as systolic and diastolic pressure >140 mmHg and/or >90 mmHg, respectively, or subject taking antihypertensive medication.
†Based on use of glucose-lowering medications and/or insulin or if fasting plasma glucose ≥126 mg/dl.
OCT, optical coherence tomography; ACS, acute coronary syndrome; HDL, high-density lipoprotein; LDL, low-density lipoprotein; LAD, left anterior descending; LCX, left circumflex; RCA, right coronary artery; AHA, American Heart Association.

Table 2. Quantitative Analysis of OCT Images

	G1 (5–8 months)	G2 (9–24 months)	G3 (25–43 months)
No. of patients	27	18	15
No. of stents	28	21	17
MLD (mm)	2.85±0.37	3.01±0.41	2.97±0.43
LA (mm^2)	6.23±1.12	6.84±1.48	6.43±1.56
SA (mm^2)	6.86±1.36	7.71±1.62	7.58±2.02
NIA (mm^2)	0.63±0.17	0.87±0.44‡	1.15±0.54*
NIT (μm)	53.4±23.9	70.1±40.6	98.6±40.2*
No. of stent struts counted	3,531	2,735	2,209
Malapposition, n (%)	49 (1.4%)	15 (0.5%)	7 (0.3%)*
Uncovered strut, n (%)	523 (14.8%)	320 (11.7%)	91 (4.1%)*,‡
Fully covered stent, n (%)	2/28 (7.1%)	1/21 (4.8%)	3/17 (17.6%)
Thrombus, n (%)	2 (7.1%)	0	1 (5.9%)

*P<0.001, G1 vs G3; †P<0.05, G1 vs G2; ‡P=0.01, G2 vs G3.
MLD, minimum lumen diameter; LA, lumen area; SA, stent area; NIA, neointimal area; NIT, neointimal thickness. Other abbreviation see in Table 1.

et al.[17] In order to validate the assessment of tissue characteristics adjacent to the stent strut, 2 observers compared the first or last cross-sectional image showing both ends of the stent and the cross-sectional image just one frame distal or proximal to the target image.

Statistical Analysis

Continuous data are expressed as means±SD. Baseline characteristics and measurements were analyzed using the Pearson chi-square test or 1-way ANOVA, as appropriate. Univariate and multivariate regression analysis was conducted to determine the independent variables for a higher rate of uncovered stent struts (more than the median value of each group). For the assessment of interobserver variability of plaque diagnosis, we calculated Cohen's kappa coefficient. Statistical analysis was performed with StatView 5.0 software (SAS Institute, Cary, NC, USA). A P value ≤0.05 was specified as the confidence level for statistical significance.

Results

Baseline Characteristics

Clinical and procedural background data for the patients classified by follow-up period are listed in **Table 1**.

Diagnostic examination was performed 5–43 months after SES implantation. The average time between stent implantation and OCT imaging follow-up was 7.1±0.8 months in the routine follow-up group (G1: 5–8 months), 13.8±3.6 months in the mid-term follow-up group (G2: 9–24 months), and 32.6±5.6 months in the long-term follow-up group (G3: 25–43 months).

No significant differences in demographic or baseline characteristics, including coronary risk factors, were found

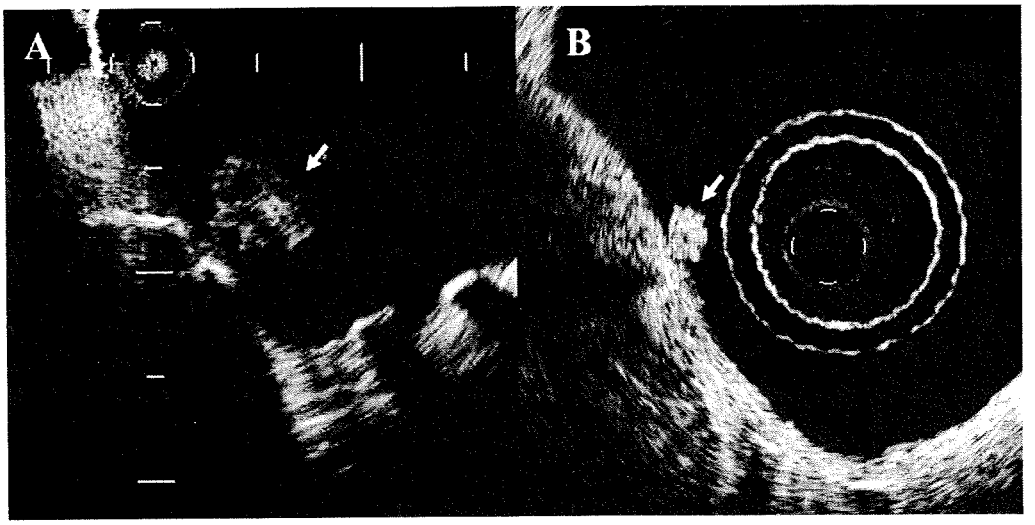

Figure 2. Thrombus formation in a sirolimus-eluting stent. (**A**) Thrombus on a stent strut not covered by neointimal tissue. (**B**) Thrombus on a stent strut covered with neointimal tissue. Arrows indicate thrombus.

Table 3. Clinical and Procedural Background and Percentage of Uncovered Stent Struts in G1

Clinical background	Rate of uncovered struts (%)	P value
Diabetes, +/–	18.7/12.0	0.018
Hypertension, +/–	15.4/14.2	0.69
Dyslipidemia, +/–	14.8/15.1	0.92
Smoking, +/–	13.9/16.6	0.39
Stent diameter, 2.5 mm/3 or 3.5 mm	18.9/11.3	0.009
Stent length, ≤18 mm/>18 mm	17.1/12.6	0.13
Stented coronary artery LAD/LCX/RCA	13.9/16.2/15.3	0.78
AHA lesion type, A/B1/B2/C	11.3/11.6/16.6/17.7	0.39

Abbreviations see in Table 1.

between groups. The treated vessel segments were distributed as follows: 30 left anterior descending lesions treated with 33 stents, 18 left circumflex lesions treated with 18 stents, and 15 right coronary artery lesions treated with 15 stents. The 3 follow-up groups did not differ significantly in terms of implanted stent diameter or length. In the present study, none of the SES exhibited angiographic restenosis as defined by more than 50% luminal loss. None of the patients in this study developed coronary events related to stent thrombosis.

Changes in Neointimal Coverage After SES Implantation

OCT findings for each follow-up period are summarized in **Table 2**. OCT images of 66 SES were obtained from 60 patients, and the total number of evaluated stent struts was 8,475 (3,531 struts in G1, 2,735 in G2, and 2,209 in G3). There were no significant differences in minimal lumen diameter, lumen area or stent area among the 3 groups. Both mean NIA and NIT increased significantly with the length of follow-up period (NIA: G1 0.63±0.17 mm^2, G2 0.87±0.44 mm^2, G3 1.15±0.54 mm^2, P=0.001; NIT: G1 53.4±23.9 μm, G2 70.1±40.6 μm, G3 98.6±40.2 μm, P<0.01). A longer follow-up was associated with a significant decrease in the percentage of incompletely apposed stent struts (G1 1.4%, G2 0.5%, G3 0.3%, P<0.01) and uncovered stent struts (G1 14.8%, G2 11.7%, G3 4.1%, P<0.01). However, even in the G3 group, only 17.6% of SES were completely covered by neointimal tissue. We observed thrombus formation on 3 stents (4.5%), even with antiplatelet therapy, 2 thrombi attached to uncovered stent struts (**Figure 2A**), and another thrombus located on the neointimal tissue over the stent strut (**Figure 2B**).

Clinical Factors Influencing Neointimal Coverage

Table 3 shows the relationship between coronary risk factors and the percentage of uncovered SES struts in the G1 patient-group. Patients with diabetes had a significantly higher percentage of uncovered stent struts than those without diabetes (19.7% vs 11.4%, P<0.01), but this percentage was not influenced by smoking, dyslipidemia, or hypertension. In both the G2 and G3 groups, clinical parameters did not correlate with the percentage of uncovered rate of SES strut (data not shown).

The relationship between procedural indices of percutaneous coronary intervention (PCI) and the percentage of uncovered stent struts in the G1 group was also examined. Small diameter stents (2.5 mm) were associated with a significantly higher percentage of uncovered struts than larger diameter stents (3.0 and 3.5 mm; 19.7% vs 10.8%, P<0.001). Complex coronary lesions (AHA type B2/C) had a higher percentage of uncovered stent struts than simple coronary lesions (AHA type A/B1), but this difference did not reach statistical significance. In the G2 group, smaller diameter stents also showed a significantly higher rate of uncovered struts compared with larger stents (15.4% vs 10.5%, P<0.05), but no procedural parameters correlated with the uncovered rate in the G3 group (**Table 3**).

Multiple linear regression analysis revealed that a smaller

Table 4. Univariate and Multivariate Analyses for Predicting Higher Rate of Uncovered Struts

	G1		G2	G3
	Univariate	Multivariate	Univariate	Univariate
Diabetes	0.02	0.85	0.90	0.43
Hypertension	0.67	–	0.87	0.69
Dyslipidemia	0.30	–	0.21	0.43
Smoking	0.15	–	0.18	0.55
Stent diameter	0.0012	0.028	0.01	0.69
Stent length	0.06	–	0.63	0.25
AHA lesion type	0.29	–	0.40	0.38

Abbreviation see in Table 1.

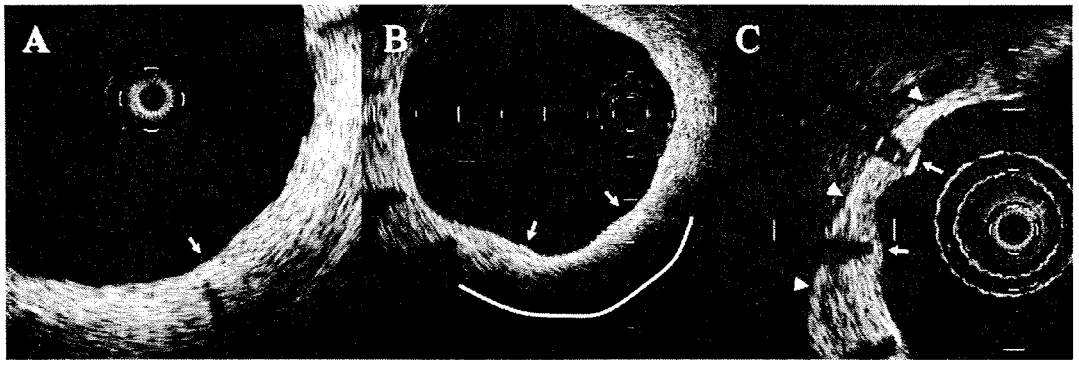

Figure 3. Representative optical coherence tomography images of vascular wall attachment to a sirolimus-eluting stent. (**A**) Fibrous tissue marked by a thickened intimal layer with a homogeneous, signal-rich texture. (**B**) Lipid-rich tissue with homogenous, diffusely bordered, signal-poor regions with overlying signal-rich bands at 5–7 o'clock (curved line indicates the region of lipid accumulation). (**C**) Calcified tissue with sharply delineated, signal-poor or signal-rich regions. Arrowheads indicate the border between fibrous tissue and calcium deposits. Arrows indicate the stent struts in each panel.

Table 5. Coronary Arterial Lesion Characteristics and Rate of Uncovered Stent Struts

	Fibrous	Lipid	Calcium
G1			
No. of stent struts	3,446	39	46
No. of uncovered struts	494	11	18
Rate of uncovered struts (%)	14.3	28.2*	39.1†
G2			
No. of stent struts	2,678	22	35
No. of uncovered struts	302	6	12
Rate of uncovered struts (%)	11.3	27.2*	34.2†
G3			
No. of stent struts	2,141	23	45
No. of uncovered struts	85	2	4
Rate of uncovered struts (%)	4.0	8.7	8.9

*P<0.05 vs Fibrous, †P<0.01 vs Fibrous.

diameter stent was an independent predictor for a higher rate of uncovered struts in the G1 group (F=5.5, P<0.001) (**Table 4**).

OCT-Based Tissue Characteristics of the Vascular Wall and Uncovered Stent Struts

Figure 3 shows representative OCT images of various tissue characteristics of the arterial wall adjacent to stent struts: a stent strut located on simple fibrous intimal layer, lipid-rich plaque or atheromatous plaque with calcium accumulation. Two observers assessed the tissue characteristics adjacent to the strut artifact and in successive images. The agreement in diagnosis of strut-containing images and successive OCT images without struts was 100% for both observers. Interobserver agreement on tissue diagnosis was 99.3% (Cohen's K value, 0.87).

Table 5 shows the relationship between the OCT-based characteristics of plaques adjacent to each stent strut and the percentage of uncovered SES. In the G1 and G2 groups this percentage was significantly higher for stent struts located on either lipid- or calcium-containing plaques than those positioned over simple fibrous plaques (G1 14.3%, 28.2%, 39.1%, respectively, P<0.01; G2 11.3%, 27.2%, 34.2%, respectively, P<0.01). By contrast, in the G3 group, the rate of uncovered stent struts tended to be higher for plaque containing lipid and calcium, but this difference did not reach statistical significance.

Discussion

We used the newly developed intravascular OCT system with an excellent spatial resolution of 10μm to visualize the very thin neointimal tissue covering SES struts, a task that was not possible with IVUS. The salient findings of the present study are that 14.8% of SES struts were not covered by neointimal tissue at 8 months after SES implantation, and that the percentage of uncovered stent struts continued to decrease by 4.1% in patients with the longest follow-up period, secondary to late neointimal growth. However, complete coverage of stent struts was achieved only in 17.6% of all implanted SES, even 32 months after implantation. Furthermore, a smaller diameter SES, the presence of underlying coronary lesions with lipid and calcium content, and diabetes correlated with delayed local neointimal coverage of the stent struts.

Late Neointimal Growth After SES Implantation

Because DESs are associated with a striking reduction in restenosis after PCI, they are routinely and widely used around the world.[18,19] However, in 2004, McFadden et al reported 4 cases of late thrombosis of a DES after discontinuation of antiplatelet therapy because of surgery or invasive endoscopic examination.[20] Their report raised general concerns about the safety of routine use of DES, because late thrombosis often results in myocardial infarction or death. Subsequently, physicians have aimed to prolong the duration of dual antiplatelet therapy,[21] because the likelihood of late stent thrombosis rises considerably with inadequate or discontinued antiplatelet therapy and delayed reendothelialization of the DES.[22,23]

Recently, Matsumoto et al used OCT to study neointimal growth over stent struts after SES implantation.[24] Although their findings were limited to observations at 6 months after implantation, they showed that the average percentage of neointima-covered struts in an individual SES was 89%, and that only 16% of implanted SES had struts fully covered by neointimal tissue. We also observed that a relatively low percentage of implanted SES was fully covered by neointima at 8 months after implantation. In the present study, we found that neointimal growth over stent struts continued for as long as 32 months after implantation, and this late neointimal growth was accompanied by a higher rate of covered SES struts and lower rate of malapposed stent struts. Such progressive decrease in the rate of uncovered SES struts seems necessary for preventing stent thrombosis, and our observations support the recent principle that longer therapy with dual antiplatelet drugs is safer. Furthermore, our observation is partly consistent with previous reports by Takano et al in which they demonstrated that 5% of SES struts were uncovered in patients for up to 24 months after SES implantation.[25,26] We were not able to confirm the plateau stage of neointimal growth after SES implantation, so we need know whether all implanted SES are completely covered at 3 years after implantation, as well as whether late neointimal growth results in angiographic restenosis at time points long after SES implantation.

Clinical Predictors for Delayed Neointimal Coverage of SES

Based on the findings of previous large DES-related clinical trials, science advisory committees of the ACC/AHA/SCAI/ACS/ADA summarized the factors relating to late stent thrombosis:[27] stenting in small vessels, multiple lesions, long stents, overlapping stents, ostial or bifurcated lesions, prior brachytherapy, suboptimal stenting result, low ejection fraction, advanced age, diabetes, renal failure, acute coronary syndrome, and premature discontinuation of antiplatelet therapy. In the present study, we found that small diameter (2.5 mm) stents, the tissue characteristics of the stented coronary segment, and diabetes were important predictors for a higher rate of uncovered struts.

The mechanisms whereby these factors suppress neointimal growth over SES struts are not clear, but tissue distribution of eluted sirolimus might play an important role. The dose of sirolimus loaded on the struts for a given length of SES is fixed, irrespective of stent diameter,[28] so the tissue concentration of sirolimus per unit area may be higher with smaller rather than larger diameter stents. Accordingly, the higher rate of uncovered struts in smaller diameter SES may be because of more significant suppression of vascular cell proliferation as compared with larger diameter SES, and this might mediate the delayed neointimal coverage of smaller SES.

Several previous studies have demonstrated the feasibility of intravascular OCT for evaluating the vascular tissue characteristics of coronary atherosclerotic plaques.[29,30] Our OCT observations revealed that neointimal growth is impaired when SES struts are deployed in coronary segments with atheromatous plaques containing either lipid or calcium, as compared with normal coronary segments or plaque consisting of simple fibrous tissue. Supporting this finding, preprocedural angiographic findings showed that complex coronary lesions (type B2/C) tended to be accompanied by a higher rate of uncovered SES in the chronic phase. These findings indicate the importance of the histopathological characteristics of coronary lesion on the healing process after SES implantation, especially with regard to neointimal formation. We assume the reason for this finding is that sirolimus inhibited smooth muscle cell proliferation more strongly in calcified or lipid plaque than in the simple fibrous plaque lesion. One explanation is the increased stiffness of the coronary artery because of complex coronary plaque, especially with calcium deposition. In the case of SES implantation in hard coronary segments, inhomogeneous distribution of the stent struts occurs because of incomplete expansion, and this may lead to an increased focal drug concentration that induces focal over-suppression of neointimal formation. Secondly, it is possible that there is a relatively small volume of viable fibrous tissue at the focal site of a complex coronary atheroma. In such complex lesions, the nonviable calcium and/or lipid content is separated by relatively thin fibrous tissue. Vascular smooth muscle cells and fibroblasts included in thin fibrous tissue are known to be the origin of proliferation and production of extracellular matrix.[31] Accordingly, the constant dose of sirolimus for a smaller volume of fibrous tissue in complex lesions might be responsible for the over-suppression of neointimal coverage of the stent struts.

Diabetes is an established risk factor for in-stent restenosis, but why diabetes correlated with a higher rate of uncovered struts in this study is unknown. Previous experimental studies have shown that hyperglycemia promotes endothelial cell apoptosis and inhibits endothelial cell proliferation.[32,33] We further speculate that the increased stiffness of the coronary arteries in diabetic patients because of the presence of complex coronary plaque, such as calcium deposition or diffuse and long atheroma distribution, is related to such divergent coronary lesions. In the complex coronary lesions of diabetes, heterogeneous tissue concentration of sirolimus would occur because of the uneven strut distribution, and might induce focal over- or under-suppression of neointimal formation over the stent struts.[28,31] The result of multivariable analysis that a small diameter stent was an independent predictor supports the concept that diabetic patients have a higher rate of uncovered strut because they often have diffuse and longer narrowing of the coronary stenosis with complex lesion characteristics.

Together with the longer follow-up period, the effects of both clinical and procedural parameters on the rate of uncovered SES struts decreased, which we assume is partly the reason for the significantly lower rate of uncovered struts in the G2 and G3 groups than in G1. This finding suggests that, irrespective of the patient's background, slow but steady growth of neointima over the struts continues in all implanted SES in the chronic phase.

Late Stent Thrombosis and Uncovered Struts of SES

None of the patients in this study experienced ischemic events after SES implantation, but 3 small thrombi inside the SES were incidentally observed, even with continued antiplatelet therapy; 2 were found on uncovered stent struts, supporting the theory that uncovered or malapposed stent struts are the primary cause of late stent thrombosis. On the other hand, 1 thrombus was located on neointimal tissue covering the stent struts, which suggests that neointimal tissue may be related to the endothelium in 2 ways: first, its margin may be lined by dysfunctional endothelial cells, and second, it may not be accompanied by an endothelial cell layer.[34,35] It is difficult to investigate these points using OCT, so further studies examining the function of neointimal tissue covering the SES struts need to be performed. On the other hand, the actual incidence of late stent thrombosis was much lower than the incidence we would expect based on the high percentage of uncovered SES struts,[36,37] and that suggests factors other than delayed endothelialization, such as the patient's hemostatic status, focal hemodynamic alterations in the implanted SES, and so on, also play an important role in the development of late stent thrombosis.[38]

Study Limitations

First, our findings were based on observations in a relatively small number of patients, and we did not use a prospective or randomized study protocol. Second, OCT is unable to image the stent struts and vascular wall in the presence of blood. Insufficient blood removal limits the application of OCT for certain coronary lesions, especially ostial and very tortuous lesions, and we were not able to assess SES that were deployed in such coronary segments. A third limitation is the resolution of OCT. Although the spatial resolution of OCT is the highest of all available intravascular imaging modalities, we might have incorrectly judged some monolayers of regenerated endothelial cells covering the stent struts as uncovered struts. Fourth, none of the enrolled patients developed cardiac events related to stent thrombosis during the observation period. Moreover, we were not able to identify factors predicting delayed neointima coverage of the SES at 24 months after implantation. Because it is reported that stent thrombosis steadily develops, even in the very late phase of SES implantation, further study with more patients should be performed in the future to clarify the relationship between the patients' background and delayed neointimal growth, as well as the development of stent thrombosis.

Conclusions

OCT imaging enabled us to visualize the thin neointimal tissue covering SES struts. Neointimal growth inside the SES progressively increased after the 8-month routine follow-up period, but complete coverage of the stent struts was established in only 17.6% of SES, even 32 months after implantation. In determining when dual antiplatelet therapy should be discontinued, the clinician should consider the patient's clinical background, especially a history of diabetes, whether or not a small diameter SES is implanted, and the tissue characteristics of the stented coronary segment.

References

1. Morice MC, Serruys PW, Sousa JE, Fajadet J, Ban Hayashi E, Perin M, et al. A randomized comparison of a sirolimus-eluting stent with a standard stent for coronary revascularization. *N Engl J Med* 2002; **346:** 1773–1780.
2. Moses JW, Leon MB, Popma JJ, Fitzgerald PJ, Holmes DR, O'Shaughnessy C, et al. Sirolimus-eluting stents vs standard stents in patients with stenosis in a native coronary artery. *N Engl J Med* 2003; **349:** 1315–1323.
3. Takano M, Mizuno K. Late coronary thrombosis in a sirolimus-eluting stent due to the lack of neointimal coverage. *Eur Heart J* 2006; **27:** 1133.
4. Karrillon GJ, Morice MC, Benveniste E, Bunouf P, Aubry P, Cattan S, et al. Intracoronary stent implantation without ultrasound guidance and with replacement of conventional anticoagulation by antiplatelet therapy: 30-day clinical outcome of the French Multicenter Registry. *Circulation* 1996; **94:** 1519–1527.
5. Urban P, Gershlick AH, Guagliumi G, Guyon P, Lotan C, Schofer J, et al; e-Cypher Investigators. Safety of coronary sirolimus-eluting stents in daily clinical practice: One-year follow-up of the e-Cypher registry. *Circulation* 2006; **113:** 1434–1441.
6. Spertus JA, Kettelkamp R, Vance C, Decker C, Jones PG, Rumsfeld JS, et al. Prevalence, predictors, and outcomes of premature discontinuation of thienopyridine therapy after drug-eluting stent placement: Results from the PREMIER registry. *Circulation* 2006; **113:** 2803–2809.
7. Eisenstein EL, Anstrom KJ, Kong DF, Shaw LK, Tuttle RH, Mark DB, et al. Clopidogrel use and long-term clinical outcomes after drug-eluting stent implantation. *JAMA* 2007; **297:** 159–168.
8. Bhatt DL, Bertrand ME, Berger PB, L'Allier PL, Moussa I, Moses JW, et al. Meta-analysis of randomized and registry comparisons of ticlopidine with clopidogrel after stenting. *J Am Coll Cardiol* 2002; **39:** 9–14.
9. Cutlip DE, Baim DS, Ho KK, Popma JJ, Lansky AJ, Cohen DJ, et al. Stent thrombosis in the modern era: A pooled analysis of multicenter coronary stent clinical trials. *Circulation* 2001; **103:** 1967–1971.
10. Pfisterer M, Brunner-La Rocca HP, Buser PT, Rickenbacher P, Hunziker P, Mueller C, et al; BASKET-LATE Investigators. Late clinical events after clopidogrel discontinuation may limit the benefit of drug-eluting stents. *J Am Coll Cardiol* 2006; **48:** 2584–2591.
11. King SB 3rd, Smith SC Jr, Hirshfeld JW Jr, Jacobs AK, Morrison DA, Williams DO, et al. 2007 Focused Update of the ACC/AHA/SCAI 2005 Guideline Update for Percutaneous Coronary Intervention: A Report of the American College of Cardiology/American Heart Association Task Force on Practice Guidelines. *Circulation* 2008; **117:** 261–295.
12. Sonoda S, Morino Y, Ako J, Terashima M, Hassan AH, Bonneau HN, et al. Impact of final stent dimensions on long-term results following sirolimus-eluting stent implantation: Serial intravascular ultrasound analysis from the Sirius trial. *J Am Coll Cardiol* 2004; **43:** 1959–1963.
13. Kataiwa H, Tanaka A, Kitabata H, Imanishi T, Akasaka T. Safety and usefulness of non-occlusion image acquisition technique for optical coherence tomography. *Circ J* 2008; **72:** 1536–1537.
14. Tanigawa J, Barlis P, Di Mario C. Heavily calcified coronary lesions preclude strut apposition despite high pressure balloon dilatation and rotational atherectomy: In-vivo demonstration with optical coherence tomography. *Circ J* 2008; **72:** 157–160.
15. Kume T, Akasaka T, Kawamoto T, Watanabe N, Toyota E, Sukmawan R, et al. Visualization of neointima formation by optical coherence tomography. *Int Heart J* 2005; **46:** 1133–1136.
16. Bouma BE, Tearney GJ. Power-efficient nonreciprocal interferometer and linear-scanning fiber-optic catheter for optical coherence tomography. *Opt Lett* 1999; **24:** 531–533.
17. Kume T, Akasaka T, Kawamoto T, Watanabe N, Toyota E, Neishi Y, et al. Assessment of coronary arterial plaque by optical coherence tomography. *Am J Cardiol* 2006; **97:** 1172–1175.
18. Morice MC, Serruys PW, Sousa JE, Fajadet J, Ban Hayashi E, Perin M, et al. A randomized comparison of a sirolimus-eluting stent with a standard stent for coronary revascularization. *N Engl J Med* 2002; **34:** 1773–1780.
19. Fajadet J, Morice MC, Bode C, Barragan P, Serruys PW, Wijns W, et al. Maintenance of long-term clinical benefit with sirolimus-eluting coronary stents: Three-year results of the RAVEL trial. *Circulation* 2005; **111:** 1040–1044.
20. McFadden EP, Stabile E, Regar E, Cheneau E, Ong AT, Kinnaird T, et al. Late thrombosis in drug-eluting coronary stents after discontinuation of antiplatelet therapy. *Lancet* 2004; **364:** 1519–1521.
21. Smith SC Jr, Allen J, Blair SN, Bonow RO, Brass LM, Fonarow GC, et al. AHA/ACC guidelines for secondary prevention for patients with coronary and other atherosclerotic vascular disease: 2006 update: Endorsed by the National Heart, Lung, and Blood Institute. *Circulation* 2006; **113:** 2363–2372.

22. Pfisterer M, Brunner-La Rocca HP, Buser PT, Rickenbacher P, Hunziker P, Mueller C, et al. Late clinical events after clopidogrel discontinuation may limit the benefit of drug-eluting stents: An observational study of drug-eluting vs bare-metal stents. *J Am Coll Cardiol* 2006; **48:** 2584–2591.
23. Joner M, Finn AV, Farb A, Mont EK, Kolodgie FD, Ladich E, et al. Pathology of drug-eluting stents in humans: Delayed healing and late thrombotic risk. *J Am Coll Cardiol* 2006; **48:** 193–202.
24. Matsumoto D, Shite J, Shinke T, Otake H, Tanino Y, Ogasawara D, et al. Neointimal coverage of sirolimus-eluting stents at 6-month follow-up: Evaluated by optical coherence tomography. *Eur Heart J* 2007; **28:** 961–967.
25. Takano M, Yamamoto M, Imai S, Murakami D, Seimiya K, Ohba T, et al. Long-term follow-up evaluation after sirolimus-eluting stent implantation by optical coherence tomography: Do uncovered struts persist? *J Am Coll Cardiol* 2008; **51:** 968–969.
26. Takano M, Xie Y, Murakami D, Inami S, Yamamoto M, Ohba T, et al. Various optical coherence tomographic findings in restenotic lesions after sirolimus-eluting stent implantation. *Int J Cardiol* 2009; **134:** 263–265.
27. Grines CL, Bonow RO, Casey DE Jr, Gardner TJ, Lockhart PB, Moliterno DJ, et al; American Heart Association; American College of Cardiology; Society for Cardiovascular Angiography and Interventions; American College of Surgeons; American Dental Association; American College of Physicians. Prevention of premature discontinuation of dual antiplatelet therapy in patients with coronary artery stents. *Circulation* 2007; **115:** 813–818.
28. Klugherz BD, Llanos G, Lieuallen W, Kopia GA, Papandreou G, Narayan P, et al. Twenty-eight-day efficacy and phamacokinetics of the sirolimus-eluting stent. *Coron Artery Dis* 2002; **13:** 183–188.
29. Kubo T, Imanishi T, Takarada S, Kuroi A, Ueno S, Yamano T, et al. Assessment of culprit lesion morphology in acute myocardial infarction: Ability of optical coherence tomography compared with intravascular ultrasound and coronary angioscopy. *J Am Coll Cardiol* 2007; **50:** 933–939.
30. Diaz-Sandoval LJ, Bouma BE, Tearney GJ, Jang IK. Optical coherence tomography as a tool for percutanous coronary interventions. *Cathet Cardiovasc Interv* 2005; **65:** 492–496.
31. Virmani R, Farb A. Pathology of in-stent restenosis. *Curr Opin Lipidol* 1999; **10:** 499–506.
32. Sheu ML, Ho FM, Yang RS, Chao KF, Lin WW, Lin-Shiau SY, et al. High glucose induces human endothelial cell apoptosis through a phosphoinositide 3-kinase-regulated cyclooxygenase-2 pathway. *Arterioscler Thromb Vasc Biol* 2005; **25:** 539–545.
33. Varma S, Lal BK, Zheng R, Breslin JW, Saito S, Pappas PJ, et al. Hyperglycemia alters PI3k and Akt signaling and leads to endothelial cell proliferative dysfunction. *Am J Physiol Heart Circ Physiol* 2005; **289:** 1744–1751.
34. Fuke S, Mackawa K, Kawamoto K, Saito H, Sato T, Hioka T, et al. Impaired endothelial vasomotor function after sirolimus-eluting stent implantation. *Circ J* 2007; **71:** 220–225.
35. Joner M, Nakazawa G, Finn AV, Quee SC, Coleman L, Acampado E, et al. Endothelial cell recovery between comparator polymer-based drug-eluting stents. *J Am Coll Cardiol* 2008; **52:** 333–342.
36. Jeremias A, Sylvia B, Bridges J, Kirtane AJ, Bigelow B, Pinto DS, et al. Stent thrombosis after successful sirolimus-eluting stent implantation. *Circulation* 2004; **109:** 1930–1932.
37. Pinto Slottow TL, Steinberg DH, Roy PK, Buch AN, Okabe T, Xue Z, et al. Observations and outcomes of definite and probable drug-eluting stent thrombosis seen at a single hospital in a four-year period. *Am J Cardiol* 2008; **102:** 298–303.
38. Buonamici P, Marcucci R, Migliorini A, Gensini GF, Santini A, Paniccia R, et al. Impact of platelet reactivity after clopidogrel administration on drug-eluting stent thrombosis. *J Am Coll Cardiol* 2007; **49:** 2312–2317.

Epithelial-Mesenchymal Transition as a Potential Explanation for Podocyte Depletion in Diabetic Nephropathy

Yukinari Yamaguchi, MD,[1] Masayuki Iwano, MD,[1] Daisuke Suzuki, MD,[2] Kimihiko Nakatani, MD,[1] Kuniko Kimura, MD,[1] Koji Harada, MD,[1] Atsushi Kubo, MD,[1] Yasuhiro Akai, MD,[1] Masao Toyoda, MD,[2] Masao Kanauchi, MD,[1] Eric G. Neilson, MD,[3] and Yoshihiko Saito, MD[1]

Background: Depletion of glomerular podocytes is an important feature of progressive diabetic nephropathy. Although the most plausible explanation for this podocyte depletion is detachment from the glomerular basement membrane after cellular apoptosis, the mechanism is unclear. Fibroblast-specific protein 1 (FSP1; encoded by the *S100A4* gene) is a member of the S100 family of calcium-binding proteins and is constitutively expressed in the cytoplasm of tissue fibroblasts or epithelial cells converted into fibroblasts by means of epithelial-mesenchymal transition.

Study Design: Retrospective cross-sectional analysis.

Settings & Participants: 109 patients with type 2 diabetes mellitus, of whom 43 (39%) underwent kidney biopsy.

Predictor: Clinical stage (4 categories) and histological grade (5 categories) of diabetic nephropathy.

Outcome: FSP1 expression in podocytes in urine and glomeruli in kidney biopsy specimens.

Measurements: Immunohistochemistry, real-time polymerase chain reaction, and in situ hybridization.

Results: 38 of 109 patients (35%) were normoalbuminuric, 16 (15%) had microalbuminuria, 8 (7%) had macroalbuminuria, and 47 (43%) had decreased kidney function. Approximately 95% of podocytes in urine sediment were not apoptotic, and 86% expressed FSP1. The number of FSP1-positive podocytes in urine sediment was significantly larger in patients with macroalbuminuria than in those with normoalbuminuria ($P = 0.03$). Intraglomerular expression of FSP1 occurred almost exclusively in podocytes from patients with diabetes, and the number of FSP1-positive podocytes was larger in glomeruli showing diffuse mesangiopathy than in those showing focal mesangiopathy ($P = 0.01$). The number also was larger in glomeruli with nodular lesions than in those without nodular lesions ($P < 0.001$). FSP1-positive podocytes selectively expressed Snail1 and integrin-linked kinase, a known trigger for epithelial-mesenchymal transition.

Limitations: Nonrepresentative study population.

Conclusions: These results suggest that the appearance of FSP1 in podocytes of patients with diabetes is associated with more severe clinical and pathological findings of diabetic nephropathy, perhaps because of induction of podocyte detachment through epithelial-mesenchymal transition–like phenomena.

Am J Kidney Dis 54:653-664.

INDEX WORDS: Podocyte; diabetes; nephropathy; epithelial-mesenchymal transition; fibroblast-specific protein 1.

Editorial, p. 590

Diabetic nephropathy is characterized by persistent proteinuria and a gradual decrease in renal function associated with thickening of the glomerular basement membrane (GBM) and expansion of the mesangial matrix, which produces progressive mesangiopathy leading to glomerulosclerosis.[1-3] Notably, these pathological changes can be attenuated by strict glycemic control and antihypertensive therapy.[4,5] Of all the histological changes in glomeruli associated with diabetic nephropathy, reduced numbers of podocytes per glomerulus are the most reliable diagnostic marker for assessing glomerular injury.[6-10]

A number of recent studies have focused on the role of podocyte depletion in the pathogenesis of proteinuria.[6-9,11] The most plausible explanation for the depletion is detachment from the

[1]From the First Department of Internal Medicine, Nara Medical University, Kashihara, Nara; [2]Department of Internal Medicine, Tokai University School of Medicine, Isehara, Kanagawa, Japan; and [3]Department of Medicine and Cell and Developmental Biology, Vanderbilt University School of Medicine, Nashville, TN.

Received October 16, 2008. Accepted in revised form May 7, 2009. Originally published online as doi: 10.1053/j.ajkd.2009.05.009 on July 21, 2009.

Address correspondence to Masayuki Iwano, MD, First Department of Internal Medicine, Nara Medical University, 840 Shijo, Kashihara, Nara 634-8522, Japan. E-mail: miwano@naramed-u.ac.jp

0272-6386/09/5404-0010$36.00/0
doi:10.1053/j.ajkd.2009.05.009

underlying GBM. Nakamura et al[12] described podocyturia as a useful marker of disease activity in diabetic nephropathy, and Vogelmann et al[13] showed that a majority of urinary podocytes are viable. Increased cellular dysfunction in the diabetic milieu and attenuation of adhesion molecules in the face of persistent glomerular hyperfiltration may be involved with podocyte detachment[14]; however, little is known about the specific mechanism.

One possibility is that podocytes become apoptotic with persistent exposure to adverse metabolic changes in diabetic plasma[10,15,16] and detach into the tubular fluid. However, only 2 studies have assessed podocyte apoptosis in human nephropathy. Kumar et al[17] showed no apoptosis in glomerular cells, whereas Verzola et al[18] showed an increase in glomerular apoptosis without quantifying the degree of podocyte apoptosis.

Another possibility is that podocytes undergo phenotypic modulation that weakens their cellular attachment in patients with diabetes. One such change might be epithelial-mesenchymal transition (EMT).[19-21] Fibroblast-specific protein 1 (FSP1; encoded by the *S100A4* gene) is a member of the S100 family of calcium-binding proteins and is constitutively expressed in the cytoplasm of tissue fibroblasts or epithelial cells converted into fibroblasts by means of EMT.[20,21] FSP1 is not simply a marker for EMT, it also has a role in determining the function of fibroblasts and has been implicated in actin rearrangement, cytoskeletal-membrane interactions, calcium sensing, and cellular growth and differentiation.[22-25] The interaction of FSP1 with cytoskeletal moieties and its early role in EMT suggests it may enable fibroblast motility.[25] In the kidney, FSP1-positive (FSP^+) cells in the tubulointerstitium are associated closely with progressive interstitial fibrosis.[21,26-31] However, little is known about intraglomerular expression of FSP1 during disease. In the present study, we examined FSP1 expression in podocytes by using renal biopsy samples and urine sediment obtained from patients with diabetic nephropathy. Our aim is to determine whether FSP1 in podocytes is associated with their detachment and the progression of diabetic nephropathy.

METHODS

Study Population

This study consecutively enrolled 109 patients (75 men, 34 women) with type 2 diabetes mellitus, who were divided into 4 groups based on urine albumin-creatinine ratio (ACR) and level of kidney function. Level of kidney function was assessed as estimated glomerular filtration rate (GFR), calculated by using the isotope dilution mass spectrometry–traceable 4-variable Modification of Diet in Renal Disease (MDRD) Study equation modified by a Japanese Society of Nephrology–Chronic Kidney Disease Initiatives coefficient[32] or estimated creatinine clearance obtained by using the Cockcroft-Gault equation.[33] In enrolled patients, normoalbuminuria was defined as urine ACR less than 30 mg/g with estimated GFR (eGFR) of 60 mL/min or greater; microalbuminuria, as urine ACR of 30 to 300 mg/g with eGFR of 60 mL/min or greater; and macroalbuminuria, as urine ACR of 300 mg/g or greater with eGFR of 60 mL/min or greater. Decreased kidney function was defined as eGFR less than 60 mL/min. Ten patients (3 men, 7 women) with renal biopsy specimens showing minimal change disease (MCD) also were enrolled as a control group. Proteinuria in patients with MCD was protein less than 2.0 g/d, and immunofluorescence microscopy showed no staining with antibodies specific for immunoglobulin G (IgG), IgA, IgM, C3, C4, or C1q.

Clinical and laboratory data for all participants are listed in Table 1. Blood pressure was measured at the time of urine collection. Glycated hemoglobin, total serum protein, serum creatinine, and urine ACR were measured within 1 month after urine collection. Every patient gave informed consent before enrollment, and our institutional review board approved the study.

Immunohistochemical Analysis of Urinary Sediment

Podocytes expressing FSP1 were detected immunohistochemically in fresh urine samples voided in the morning. Podocyte in urine sediment were counted by using a modification of the method of Hara et al.[12,13,34-36] Ten milliliters of freshly voided urine was centrifuged at 700*g* for 5 minutes. The supernatant then was decanted and the pellet was resuspended in 1 mL of phosphate-buffered saline (PBS), followed by centrifugation onto glass slides using a Cytospin Cytocentrifuge (Shandon Inc, Pittsburgh, PA). The slides were then air dried and fixed with 4% paraformaldehyde for 15 minutes at 4°C. After washing 3 times with PBS, slides were incubated with Protein Block Serum-Free (DakoCytomation Inc, Carpinteria, CA) for 30 minutes at room temperature. Each sample then was incubated for 60 minutes with mouse anti–human podocalyxin monoclonal antibody (PHM5; 1:200 dilution; Australian Monoclonal Development, Artamon, NSW, Australia) and rabbit polyclonal anti–human FSP1 antibody[20] (1:500 dilution). After washing 3 times with PBS, slides were incubated for 30 minutes with Cy3-conjugated goat anti–mouse IgG antibody (1:1,000 dilution; Jackson ImmunoResearch Laboratories Inc, West Grove, PA) and Cy2-conjugated donkey anti–rabbit IgG antibody (1:500 dilution; Jackson ImmunoResearch). Finally, slides were counterstained with 4′6-diamidine-2′-phenylindole dihydrochloride (DAPI; Molecular Probes Inc, Eugene, OR) and viewed under a fluorescence microscope (Axiovert 2000; Carl Zeiss, Oberkochen, Germany).

Synaptopodin and CD68 also were used to examine urinary podocytes and hematopoietic cells. Each sample of centrifuged urinary cells was incubated for 60 minutes with

cell by using a cytospin procedure, then detected immunocytochemically. By also staining for the podocyte marker podocalyxin, podocytes can be detected. A representative podocalyxin$^+$/FSP1$^+$ cell is shown in Fig 1. We counted podocalyxin$^+$ and podocalyxin$^+$/FSP1$^+$ cells in each urine sediment. We did not count podocalyxin$^+$ cells with diameters less than 15 μm. This was to exclude CD68$^+$ monocytes, which express podocalyxin, but have diameters less than 15 μm (data not shown).[40] Podocalyxin also is expressed by extraglomerular endothelial cells in the kidney,[41,42] but no podocalyxin$^+$ cell expressed the endothelial marker CD31 (data not shown). Detectable FSP1 staining was seen in 86% of urinary podocytes from the total cohort of patients with diabetes. Assessed by means of DAPI staining, 95% of FSP1$^+$ podocytes were not apoptotic. We also identified urinary podocytes by using synaptopodin as a podocyte marker and found that 91% of urinary synaptopodin$^+$ podocytes expressed FSP1. Thus, about 90% of detached podocytes were not apoptotic and expressed FSP1.

Total numbers of podocytes (podocalyxin$^+$ cells) were significantly greater in patients with diabetes than in those with MCD ($P < 0.001$; Fig 2A), as were numbers of podocalyxin$^+$/FSP1$^+$ podocytes ($P < 0.001$). Percentages of podocytes positive for FSP1 were 86% in patients with diabetes and 66% in patients with MCD. The total number of podocytes was also significantly greater in patients with macroalbuminuria than in those with normoalbuminuria ($P = 0.01$; Fig 2B). Likewise, the number of podocalyxin$^+$/FSP1$^+$ podocytes in urine sediment was significantly greater in patients with macroalbuminuria than in those with normoalbuminuria ($P = 0.03$). However, the percentage of FSP1$^+$ podocytes was about the same in the different groups (84.3% in normoalbuminuria, 86.1% in microalbuminuria, 86.4% in macroalbuminuria, and 86.1% in decreased kidney function). Numbers of FSP1$^+$ podocytes significantly correlated with levels of proteinuria ($r = 0.35$; $P < 0.001$). Finally, there were fewer FSP1$^+$ podocytes in urine sediment from patients with reduced renal function than in those with microalbuminuria. In another analysis, we categorized patients with diabetes into 4 groups based on estimated creatinine clearance,

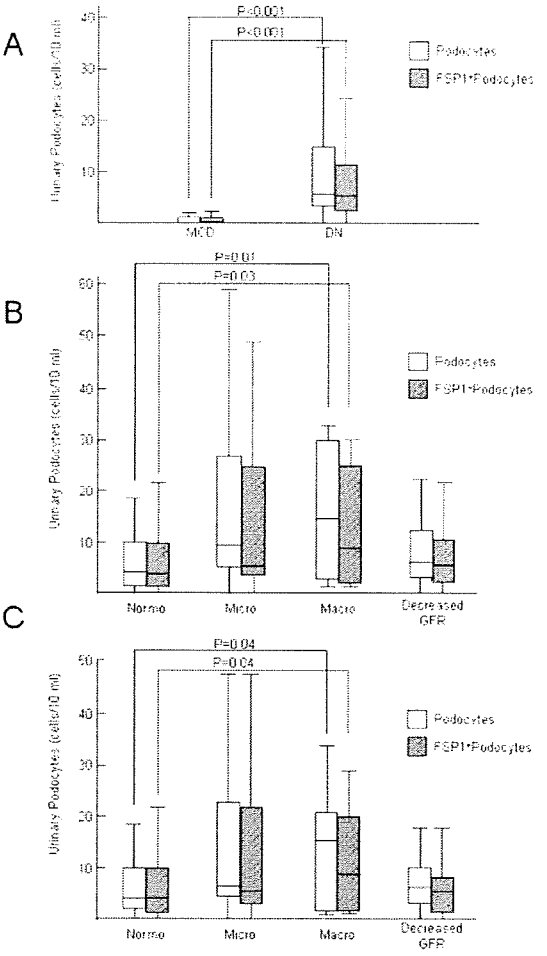

Figure 2. Quantitative analysis of urinary podocytes. (A) Numbers of urinary podocytes (podocalyxin-positive [$^+$] cells) (open box) and fibroblast-specific protein 1 (FSP1)$^+$ podocytes (closed box) in patients with minimal change disease (MCD) and diabetic nephropathy (DN). (B, C) Numbers of urinary podocytes (podocalyxin$^+$ cells; open box) and FSP1$^-$ podocytes (closed box) in the 4 groups of patients with DN (normoalbuminuric [normo], microalbuminuric [micro], macroalbuminuric [macro], decreased kidney function defined as a glomerular filtration rate [GFR] < 60 mL/min). (B) GFR was estimated by using the Modification of Diet in Renal Disease (MDRD) Study equation modified with the Japanese coefficient. (C) Creatinine clearance was estimated using the Cockcroft-Gault formula.

calculated by using the Cockcroft-Gault formula. Results were similar, as shown in Fig 2C.

Localization of FSP1 in Renal Biopsy Specimens

We used synaptopodin, ZO-1, and GLEPP1 as markers to identify podocytes in frozen sections of renal biopsy specimens (Fig 3). Almost all FSP1$^+$ cells within diabetic glomeruli expressed

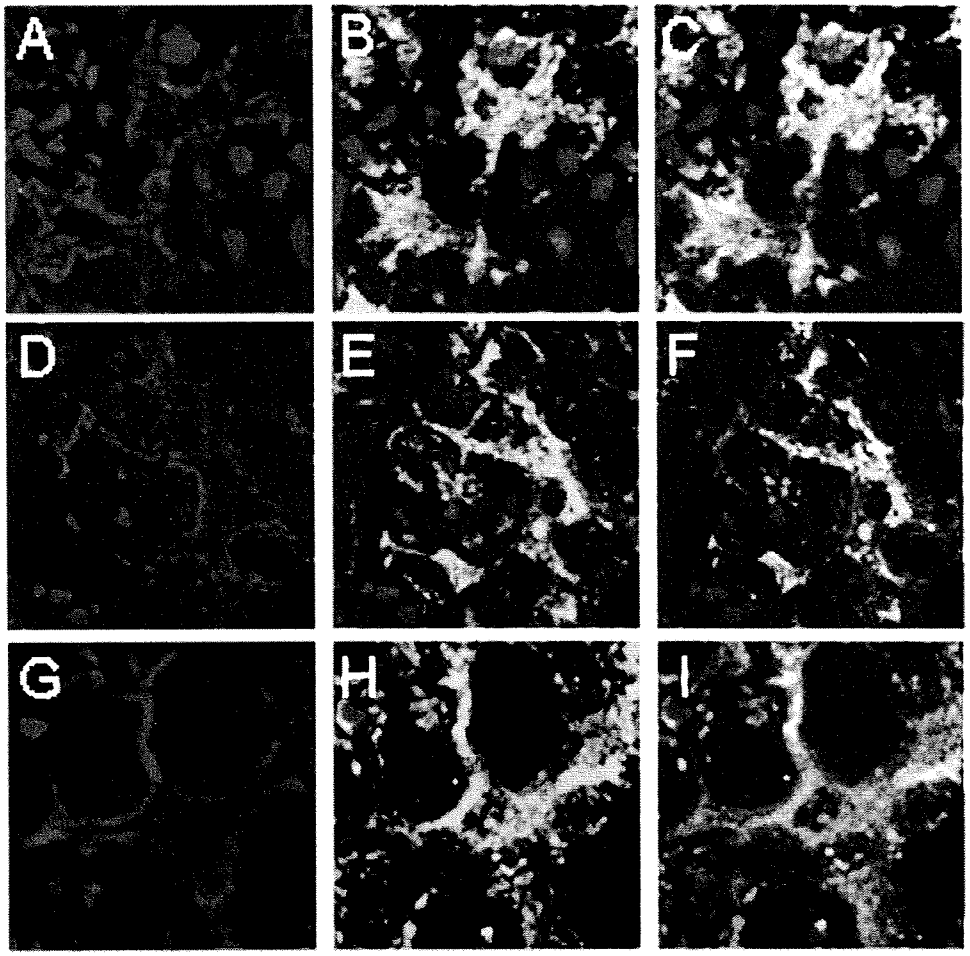

Figure 3. Representative immunofluorescence evaluation of a renal biopsy specimen from a patient with diabetic nephropathy. (A, D, G) Synaptopodin, zona occludens 1 (ZO-1), and glomerular epithelial protein 1 (GLEPP1) serve as markers of podocytes (red staining), respectively. (B, E, H) Cells expressing fibroblast-specific protein 1 (FSP1) (green staining) are clearly present within diabetic glomeruli. (C, F, I) Merged images show colocalization of podocyte markers and FSP1, confirming that some podocytes express FSP1 in diabetic glomeruli. Nuclei were stained with DAPI (4'6-diamidine-2'-phenylindole dihydrochloride; blue). (Original magnification ×400.)

synaptopodin, ZO-1, and GLEPP1, but only a fraction of the synaptopodin$^+$/ZO-1$^+$/GLEPP1$^+$ podocytes expressed FSP1; that is, all cells expressing FSP1 within glomeruli were podocytes, but not all podocytes expressed FSP1 (Fig 3A to I). FSP1$^+$ cells were not observed within MCD glomeruli (Fig S1; provided as online supplementary material available with this article at www.ajkd.org).

We also confirmed FSP1 expression by podocytes by using in situ hybridization; mRNA encoding FSP1 was expressed in podocytes in patients with diabetic nephropathy (Fig 4A), but not in podocytes of patients with MCD (Fig 4B). Glomerular expression of FSP1 mRNA analyzed by means of laser-capture microdissection and real-time PCR showed that glomerular FSP1 expression was significantly upregulated in diabetic nephropathy (Fig 4C).

Histological Grade of Diabetic Nephropathy and Numbers of FSP1$^+$ Podocytes in Renal Biopsy Specimens

Dual-labeling studies showing the glomerular distribution of FSP1 and collagen type IV show progressive mesangiopathy and nodular sclerosis with increasing grade (Fig 5). FSP1$^+$ podocytes were present on the outer side of the GBM. Some FSP1$^+$ podocytes appear to have detached from the GBM in grade 4 glomeruli, although an

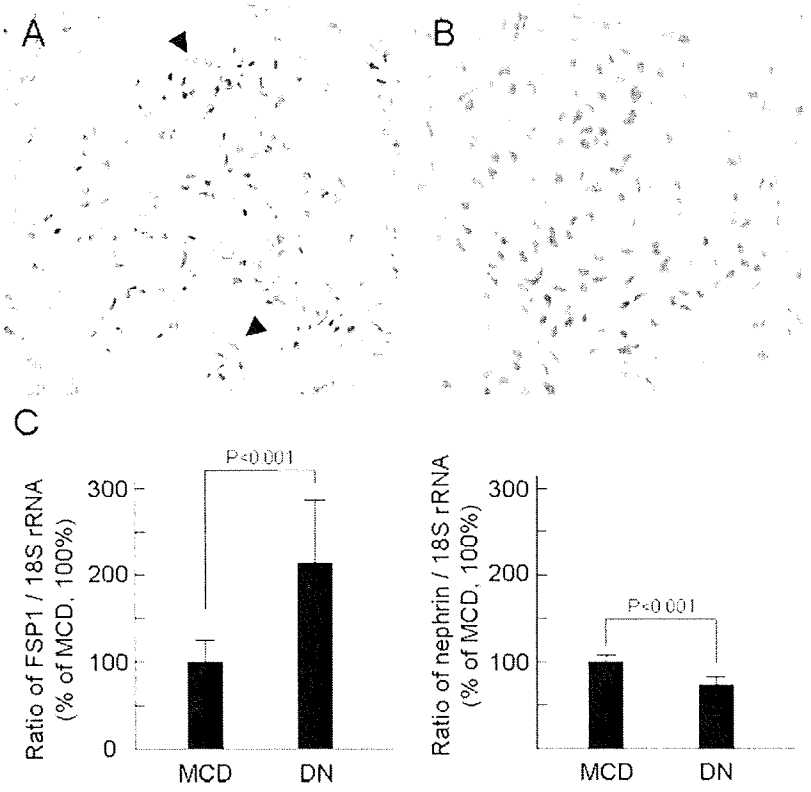

Figure 4. Detection of fibroblast-specific protein 1 (FSP1) messenger RNA (mRNA) by using in situ hybridization and reverse-transcription polymerase chain reaction (PCR). (A) FSP1 mRNA was expressed predominantly in podocytes (arrow) from patients with diabetic nephropathy (DN). (B) FSP1 mRNA was not detected in sections from patients with minimal change disease (MCD). (Original magnification ×200.) (C) Levels of glomerular FSP1 mRNA from laser-capture microdissection samples measured by using real-time PCR normalized to 18S ribosomal RNA (rRNA) were significantly greater in DN than MCD (left graph). Levels of glomerular nephrin mRNA normalized to 18S were significantly lower in DN than MCD samples (right graph).

artifact stemming from the angle of sectioning cannot be ruled out (Fig 5B). Numbers of $FSP1^+$ podocytes from patients with each grade of diabetic nephropathy and MCD are listed in Table 2. In patients with MCD or in normal glomeruli obtained from nephrectomy, the number of $FSP1^+$ podocytes per glomerular profile was less than for grade 1 glomeruli ($P < 0.001$). In grade 2 glomeruli, the number of $FSP1^+$ podocytes per glomerular profile was significantly larger than in grade 1 glomeruli ($P = 0.007$), and in grades 3 and 4 glomeruli, numbers of $FSP1^+$ podocytes per glomerular profile were significantly larger than in grade 2 ($P < 0.001$). Thus, the number of $FSP1^+$ podocytes per glomerular profile increased with the severity of mesangiopathy and the development of nodular lesions. However, a marked decrease in $FSP1^+$ podocytes was seen at diabetic grade 5 compared with the other groups, which may reflect prior detachment. When we also counted glomerular podocytes in the same sections, we found that podocyte numbers decreased with the severity of mesangiopathy and development of nodular lesions (Table 2). This reciprocal change in numbers of $FSP1^+$ and glomerular podocytes suggests that EMT may explain the loss of podocytes in diabetes. As reported previously, FSP1 also was localized in interstitial fibroblasts, circulating fibroblasts in the capillary lumen, and tubular epithelial cells undergoing EMT (data not shown).[21,29]

Podocyte Expression of EMT Markers in Diabetic Nephropathy

We next examined the expression of EMT markers in podocytes in biopsy specimens from patients with diabetic nephropathy. ZO-1 is a membrane protein localized at tight junctions, and its loss is a standard marker of EMT. As shown in Fig 6A to C, glomerular $FSP1^+$/ZO-1–negative cells are more common at advanced stages (corresponding to grade 4 in Fig 5A) of diabetic nephropathy than in earlier stages (compare Fig 6C with Fig 3F). In contrast, Snail1, a zinc-finger transcription factor that represses the expression of various adherens and tight junction proteins,[19,29,43] was observed in podocytes at early stages (grade 2 in Fig 5A) of diabetic nephropathy (Fig 6D to I). No Snail1 was observed in podocytes from patients with MCD

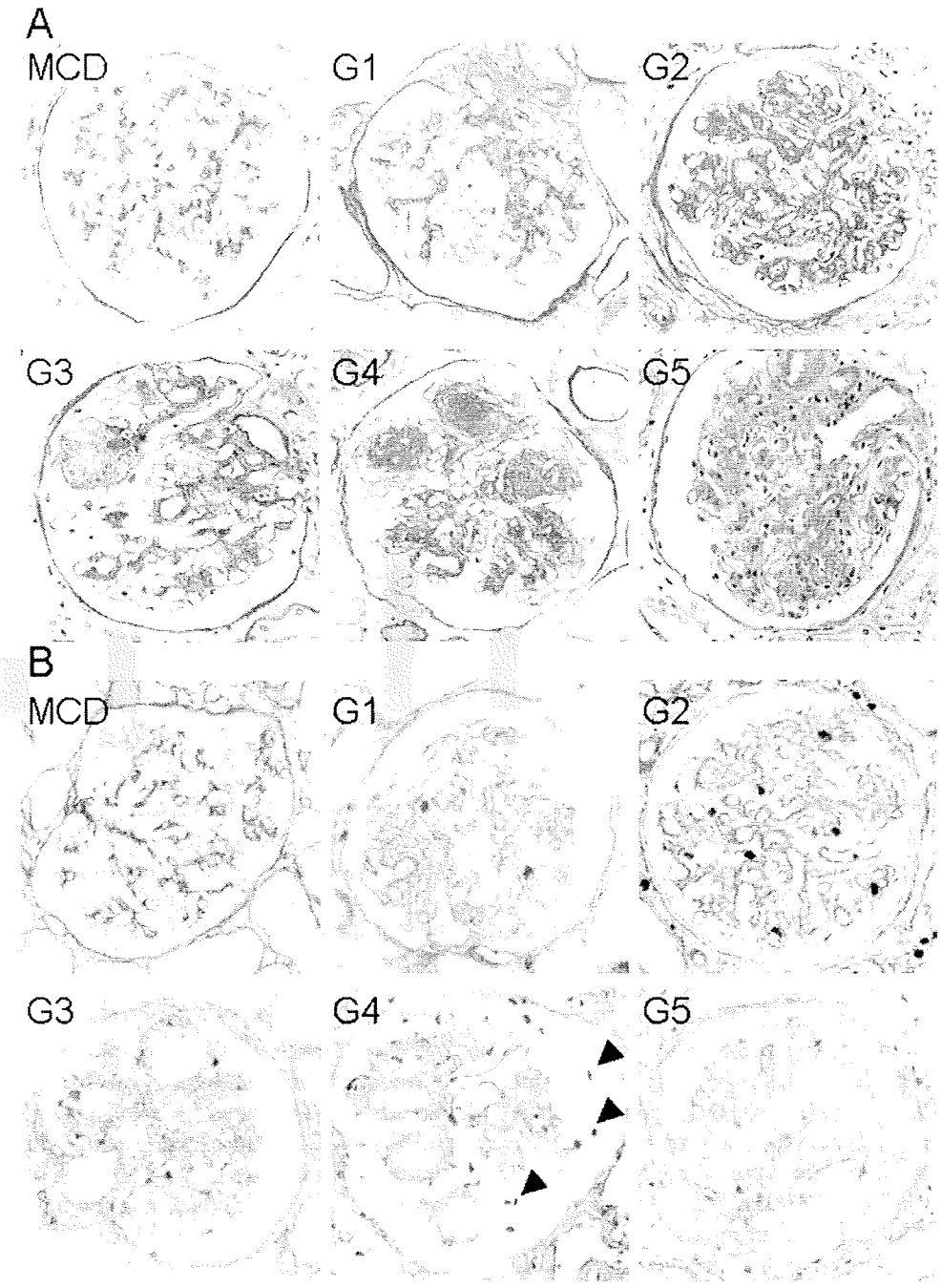

Figure 5. Representative glomeruli of different histological grades of diabetic nephropathy. (A) Periodic acid–Schiff staining of representative glomeruli in renal biopsy sections from patients with minimal change disease (MCD) and each histological grade (G1 to G5) of diabetic nephropathy. (Original magnification ×200.) (B) Immunohistochemical detection of fibroblast-specific protein 1 (FSP1; purple) and collagen type IV (brown) in renal biopsy sections from patients with MCD and each histological grade (G1 to G5) of diabetic nephropathy (all sections were stained with both anti-FSP1 and anti–collagen type IV antibodies). FSP1-positive (FSP1$^+$) podocytes (purple) at G1 to G3 are localized to the outside of the glomerular basement membrane. FSP1$^+$ cells at G4 are drifting into Bowman space (arrowheads) as detached podocytes. (Counterstain is nuclear fast red; original magnification ×200.)